Video Article

Fabrication of Fine Electrodes on the Tip of Hypodermic Needle Using Photoresist Spray Coating and Flexible Photomask for Biomedical Applications

Joho Yun[1], Jinhwan Kim[2], Jong-Hyun Lee[1,2]

[1]Department of Biomedical Science and Engineering, Gwangju Institute of Science and Technology (GIST)

[2]School of Mechanical Engineering, Gwangju Institute of Science and Technology (GIST)

Correspondence to: Jong-Hyun Lee at jonghyun@gist.ac.kr

URL: https://www.jove.com/video/56622
DOI: doi:10.3791/56622

Keywords: Neuroscience, Issue 129, Hypodermic needle, interdigitated electrodes, spray coating, flexible film photomask, electrical impedance spectroscopy, EIS

Date Published: 11/28/2017

Citation: Yun, J., Kim, J., Lee, J.H. Fabrication of Fine Electrodes on the Tip of Hypodermic Needle Using Photoresist Spray Coating and Flexible Photomask for Biomedical Applications. *J. Vis. Exp.* (129), e56622, doi:10.3791/56622 (2017).

Abstract

We have introduced a fabrication method for electrical impedance spectroscopy (EIS)-on-a-needle (EoN: EIS-on-a-needle) to locate target tissues in the body by measuring and analyzing differences in the electrical impedance between dissimilar biotissues. This paper describes the fabrication method of fine interdigitated electrodes (IDEs) at the tip of a hypodermic needle using a photoresist spray coating and flexible film photomask in the photolithography process. A polyethylene terephthalate (PET) heat shrink tube (HST) with a wall thickness of 25 μm is employed as the insulation and passivation layer. The PET HST shows a higher mechanical durability compared with poly(p-xylylene) polymers, which have been widely used as a dielectric coating material. Furthermore, the HST shows good chemical resistance to most acids and bases, which is advantageous for limiting chemical damage to the EoN. The use of the EoN is especially preferred for the characterization of chemicals/biomaterials or fabrication using acidic/basic chemicals. The fabricated gap and width of the IDEs are as small as 20 μm, and the overall width and length of the IDEs are 400 μm and 860 μm, respectively. The fabrication margin from the tip (distance between the tip of hypodermic needle and starting point of the IDEs) of the hypodermic needle is as small as 680 μm, which indicates that unnecessarily excessive invasion into biotissues can be avoided during the electrical impedance measurement. The EoN has a high potential for clinical use, such as for thyroid biopsies and anesthesia drug delivery in a spinal space. Further, even in surgery that involves the partial resection of tumors, the EoN can be employed to preserve as much normal tissue as possible by detecting the surgical margin (normal tissue that is removed with the surgical excision of a tumor) between the normal and lesion tissues.

Video Link

The video component of this article can be found at https://www.jove.com/video/56622/

Introduction

Hypodermic needles are widely utilized in hospitals for biopsies and drug delivery because they are inexpensive and easy to use. They also have excellent mechanical properties despite their thin diameter and a sharp-edged structure suitable for invasion. During a biopsy, the target tissues are sampled in the hollow of the hypodermic needle with ultrasonography guidance[1]. Although ultrasonography is free of radiation, safe for fetuses and pregnant women, and provides real-time imaging, it is difficult to see organs that are deep within the body, especially in the case of obese patients because ultrasonic waves cannot penetrate air or fat tissues[2]. In addition, a surgeon cannot acquire depth information from the two-dimensional ultrasonography that is conventionally utilized in the majority of hospitals, resulting in the need for multiple biopsies if physicians lack skill or experience. In drug delivery for spinal anesthesia, physicians determine that the needle has reached the spinal space if the cerebrospinal fluid (CSF) flows backward into the syringe while carefully inserting the needle into the patient's back. After confirming the reflux of CSF, the anesthesia drug is injected into the spinal space[3]. However, physicians risk penetrating or cutting off nerve fibers in the spinal space, causing severe pain to patients and even paraplegia[4,5]. Thus, this procedure also requires a skillful physician. One solution to overcome and mitigate the aforementioned difficulties is to add a navigation function to the hypodermic needle so that objective information on the needle's position can be provided. This would help a physician readily perform a biopsy, drug delivery, and even a surgery without relying on their empirical judgment only.

In order to electrically localize the target tissues in the body, a hypodermic needle incorporating an electrical impedance spectroscopy (EIS) sensor has been introduced as EIS-on-a-needle (EoN)[6]. The EIS sensor is currently utilized in the field of biomedical engineering for applications such as DNA detection[7,8,9], bacteria/virus detection[10,11,12], and analysis on cells/tissues[13,14,15,16,17,18,19,20,21,22]. The EoN can discriminate between dissimilar materials in a frequency domain based on their electrical conductivity and permittivity. The discrimination capability of the EoN was verified for various concentration levels of phosphate buffered saline (PBS)[23], porcine fat/muscle tissues[6,23], and even human renal normal/cancer tissues[24,25]. This capability of the EoN is expected to considerably increase the biopsy accuracy by locating the target tissues based on the differences in electrical impedance between the target lesion tissues and the neighboring normal tissues. In a similar manner, investigating

differences in the electrical impedance between the drug injection space (spinal or epidural space) and surrounding tissues can help physicians deliver an anesthesia drug at the exact target location. Furthermore, the EoN can be utilized to electrically stimulate the brain/muscle as well as to determine an optimal surgical margin during surgeries that involve the partial resection of a tumor, such as partial nephrectomy, to preserve as much normal tissue as possible.

One of the biggest challenges in the realization of the EoN is the fabrication of electrodes on the curved surface of a hypodermic needle having a small radius of curvature. Direct metal patterning using a conventional photolithography process has been regarded as unsuitable for the fabrication of micro-sized electrodes on a curved substrate with a diameter of several millimeters or less. So far, various methods, including conformal printing[26], flexible dry film photoresist[27], the microfluidic method[28], nanoimprint lithography[29], and substrate-rotating lithography[30], have been introduced to fabricate metal/polymer patterns on a curved surface. However, there are still limitations due to the EoN requirements, such as the required substrate with a diameter of less than 1 mm, total electrode length of 20 mm or more, width and gap of electrodes ranging in tens of micrometers, and high volume production.

In the present study, direct metal patterning by employing photoresist spray coating and a flexible film photomask is proposed to realize micro-sized electrodes on the curved surface of a hypodermic needle. The diameter of the needle is as small as 720 µm (22-gauge), which is widely used for biopsies and drug delivery in hospitals. The production yield of the proposed fabrication method is also evaluated to determine the feasibility of bulk production at an affordable price.

Protocol

1. Electrical Insulation of Hypodermic Needle

NOTE: A transparent heat shrink tube (HST) is employed for the electrical insulation of a hypodermic needle that is 720 µm in diameter and 32 mm in length. The HST is made of polyethylene terephthalate (PET), which shows good chemical resistance to most acids and bases, excellent mechanical durability, and biocompatibility. The initial inner diameter and wall thickness of the HST are 840 µm and 25 µm, respectively. The diameter of the HST tends to be reduced by more than 50% at a temperature of 100 °C, with even greater reduction at higher temperatures up to 190 °C. Note that PET HST is a thermosetting material that has the property of becoming permanently hard and rigid when cured. The size of the hypodermic needle and shrink tube can be adjusted depending on the research purpose and applications. The overall fabrication process is graphically summarized in **Figure 1**.

1. Cut the HST to a length of 3 cm. Adjust the length of the tube depending on the penetration depth of the hypodermic needle.
2. Insert the hypodermic needle into the cut HST.
3. Shrink the tube using a heat gun at a temperature of 150 °C, which is set to prevent unwanted additional contraction when dehydration is carried out at 105 °C in the cleaning process (in step 1.6).
4. Separate the hypodermic needle from its hub.
5. Clean the hypodermic needle insulated by the HST in a deionized (DI) water bath (20 °C) with ultrasonic agitation at 30 kHz and 350 W power.
6. Dehydrate the hypodermic needle insulated by the HST on a hotplate at 105 °C for 10 min.

2. Au Deposition Using Sputtering

NOTE: In this study, the sputtering process that is available is used to deposit an Au layer for electrodes, although an e-beam evaporation process can be an alternative method. It has been confirmed that the temperature rise induced in the sputtering process rarely causes additional shrinkage of the HST. However, a process that continues for more than several minutes might heat the HST above the initial shrinkage temperature. This can cause additional shrinkage of the HST, resulting in an increase in the fabrication margin from the tip.

1. Arrange the cleaned hypodermic needles insulated by the HST side by side on a glass slide using double-sided tape for Cr/Au deposition.
2. **Using sputtering equipment, deposit Cr/Au on the cleaned hypodermic needles insulated by the HST.**
   NOTE: In this case, the thicknesses of Cr and Au were 10 nm and 100 nm, respectively (Cr was used for the adhesion layer between the HST and the Au layer).
   1. Arrange as many needles as possible in order to reduce production cost and production time. Use the sputtering conditions below to deposit 10 nm Cr and 100 nm Au.
   2. For Cr sputtering, set Cr target diameter: 4 inch, RF power: 300 W, argon pressure: 5 mTorr, and shutter open time: 20 s (10 nm).
   3. For Au sputtering, use Au target diameter: 4 inch, DC power: 300 W, argon pressure: 10 mTorr, and shutter open time: 80 s (100 nm).

3. Spray Coating

NOTE: A low-viscosity (14 cp) photoresist is used in the spray coating process to increase spray efficiency. The photoresist can be easily coated on the Au-sputtered needle only when the needle is heated.

1. Fix one of the Au-sputtered hypodermic needles on a glass slide using double-sided tape.
2. Place the slide glass on a chuck of the spray coater that is being heated at 100 °C. Wait 2 - 3 min until the needle is sufficiently heated.
3. Spray the photoresist on the Au-sputtered needle while heating the needle at 100 °C. Perform the spray-coating process using the following conditions. Set nozzle diameter: 400 µm, nozzle moving speed: 70 mm/s, spray pressure: 500 kPa, and distance between chuck and nozzle: 13.5 cm.
4. After spray coating is finished, leave the glass slide on the chuck at 100 °C for 3 min to perform a soft baking process.

5. Inspect the result using a microscope set to 100X magnification to determine whether the photoresist is uniformly coated on the Au-sputtered needle.

4. UV Exposure and Developing

NOTE: In general, prior to UV exposure, a flexible film photomask is attached to a flat transparent plate to remove the air gap between the photomask and the sample to be exposed to UV light. However, in this study, the photomask is used without the flat transparent plate to realize direct metal patterning on the curved surface of the hypodermic needle. The photomask can conformably bent along the curve of the hypodermic needle to achieve the best patterning resolution feasible with the contact aligner. The bending allows the flexible photomask to keep the contact area between the photomask and the curved surface of the hypodermic needle as large as possible. Taking a wet etching process (not a lift-off process) for metal patterning into consideration, the use of a positive photoresist is more advantageous than the use of a negative photoresist. This is because the entire area except the electrode pattern is transparent, thereby providing a wide field of view to readily align the electrode pattern with the center of the needle.

1. **To minimize wedge error, slowly lift a freely movable sample-holding plate until it fully contacts the fixed photomask-holding plate. Then, fix the sample-holding plate using a pneumatic pump.**
    1. Carry out this process to possibly avoid undesirable patterns, which may be formed by the scattering of UV light in the air gap, and caused by the incomplete contact between the sample and photomask.
    NOTE: In addition, the minimization of wedge error ensures that the photoresist-coated hypodermic needle does not move when it contacts a film photomask in the next alignment step, even though the contact surface of the hypodermic needle has a round shape.

2. Place the photoresist-coated hypodermic needle on the sample-holding plate of the aligner.
3. **Align the projected image of the photoresist-coated hypodermic needle with the alignment pattern of the film photomask.**
NOTE: In this case, the alignment pattern of the film photomask was designed as two parallel lines at a distance of 800 µm, considering the thickness of the HST and coated photoresist.
    1. Align two boundary lines of the projected image with two parallel alignment lines of the photomask (**Figure 1e**); thus, the photoresist-coated hypodermic needle can be positioned at the center of two parallel alignment lines, with an alignment error of 10 µm or less.
    2. Monitor the alignment process in real-time through the display monitor connected to the charge-coupled device (CCD) camera and microscope.

4. Bring the photoresist-coated hypodermic needle into contact with the fixed flexible photomask by slowly lifting the needle towards the photomask.
5. Carry out UV exposure for 30 s (UV intensity: 15 mJ/cm^2) and follow this by the developing process for 3 min.
6. Rinse the developer out of the sample using DI water.
7. Inspect the result through a microscope set to 200X magnification to determine whether the photoresist is clearly patterned on the Au-sputtered hypodermic needle. If the exposed photoresist is not perfectly removed after the developing process, repeat the developing process at 30 s intervals.

5. Cr/Au Wet Etching

CAUTION: Avoid skin/eye contact with the Cr and Au wet etchants.

1. Use a tweezer to detach the sample (photoresist-patterned hypodermic needle) fixed on the glass slide.
2. Immerse the sample into the Au wet etchant for 1 min.
3. Rinse the Au etchant out of the sample using DI water.
4. Inspect the result through a microscope set to 200X magnification. If the gold to be removed still remains, repeat the wet etching process at 10 s intervals. Excessively long wet etching time makes the interdigitated electrode (IDE) thinner.
5. Immerse the sample into the Cr etchant for 30 s.
6. Rinse the Cr etchant out of the sample using DI water.

6. Removal of Residual Photoresist and Passivation

1. Immerse the sample (metal-patterned hypodermic needle) into an acetone solution for 1 min.
2. Rinse the sample with DI water and dehydrate it on a hot plate at 105 °C for 10 min.
3. For electrical passivation of the connection lines, cut the shrink tube so that it is 2 - 3 mm longer than the electrode (20 mm, the maximum depth to penetrate), as shown in **Figure 2**, because the length of the HST will be reduced after the HST shrinks.
4. After positioning the HST as far as possible from the end of the IDE, raise the temperature of the HST using a heat gun at 150 °C to tightly passivate the needle.

Representative Results

The interdigitated electrodes (IDEs), as shown in **Figure 2**, result in a larger effective sensing area on a limited surface compared to other shapes of electrodes. The overall length of the IDEs is designed to be 860 µm to detect and analyze the impedance changes at less than 1 mm intervals in the biotissues, which will provide a high locating accuracy in biopsy and drug delivery procedures. The total width of the IDEs is 400 µm, which is a geometrically feasible dimension on the curved surface of the hypodermic needle when using the proposed photolithography process. Both the gap and width of the IDEs are as small as 20 µm, which is close to the minimum dimensions of a commercially available film photomask. The maximum penetration depth of the EoN into biotissues is designed to be 20 mm, considering thyroid/prostate biopsies and spinal anesthesia. The total length of the EoN can be adjusted depending on the application.

As shown in **Figure 3**, the IDEs are successfully fabricated at the tip of the hypodermic needle with a diameter of 720 µm. Overdose during UV lithography was required to compensate for the UV dose imbalance arising from imperfect contact between the outer portion of the photomask and the curved surface of the hypodermic needle. This will increase the gap and decrease the width of the IDEs in the case of a positive photoresist. To resolve the adverse effect of the dimensional changes, the width and the gap were intentionally designed to be 25 µm and 15 µm on the photomask, respectively. Thereby, both the width and the gap of the IDEs can be successfully fabricated to be 20 µm by optimizing the UV exposure time. The fabrication margin from the tip of the hypodermic needle is as small as 680 µm, which will avoid unnecessarily excessive invasion into biotissues during the electrical impedance measurement. A PET HST was employed as the electrical insulation layer for both the IDEs and the connection lines, and also as the electrical passivation layer for the connection lines. The HST features low electrical conductivity/permittivity, durable mechanical properties compared to a poly(p-xylylene) polymer coating, chemical resistance to most acids and bases, and biocompatibility.

From the standpoint of mechanical durability, device failure (for instance, the insulation layer, passivation layer, and/or electrodes peeling off) was not observed even after penetration into biotissues more than 100 times, whereas a poly(p-xylylene) polymer with a wall thickness of 1.5 µm did not endure penetration into porcine tissues more than 20 times. This indicates that the PET HST showed strong adhesion with the sputtered electrodes as well as high durability for clinical trials. Furthermore, the HST shows good chemical resistance to most acids and bases, which enables the EoN to detect the electrical properties of various kinds of chemicals or biomaterials and keeps the HST durable during electrochemical deposition of Au electrodes using acid solution (H_2SO_4). In the electrochemical deposition process, the Au electrode layer tends to grow in fractal structures, which allows the effective area of the sensing electrodes to significantly increase on the limited surface area of the needle to achieve a higher sensitivity.

To evaluate the discrimination capability of the EoN and its depth profiling capability into biotissue, various concentration levels of PBS and four-layered porcine tissue were employed, respectively[23]. The impedance analyzer was connected to both the EoN and a laptop, as shown in **Figure 4**. To carry out depth profiling into the four-layered porcine tissue, the EoN was fixed to the height controller, with a resolution of 10 µm. The various concentration levels of PBS were prepared as 1x, 0.5x, 0.25x, 0.125x, and 0.0625x, by serially diluting the 1x PBS with DI water. The lengths of the IDEs and connection lines used in the experiment was 300 µm and 28 mm, respectively. As shown in **Figure 5a**, the EoN could successfully discriminate various concentration levels of PBS. Because the 1x PBS was diluted serially with DI water, the electrical conductivity of diluted PBS decreased because of the very small conductivity of DI water. Thus, the magnitude of impedance increased as the concentration level of PBS decreased. Based on the discrimination capability of EoN, the depth profiling of the four-layered porcine tissue was carried out at the frequency of 1 MHz, which was decided as the optimal frequency in our previous research. The EoN was inserted into the four-layered porcine tissue at increments of 1 mm. As shown in **Figure 5b**, the magnitude of impedance measured from fat tissue was clearly discriminated from that of muscle tissue, according to the penetration depth of the EoN.

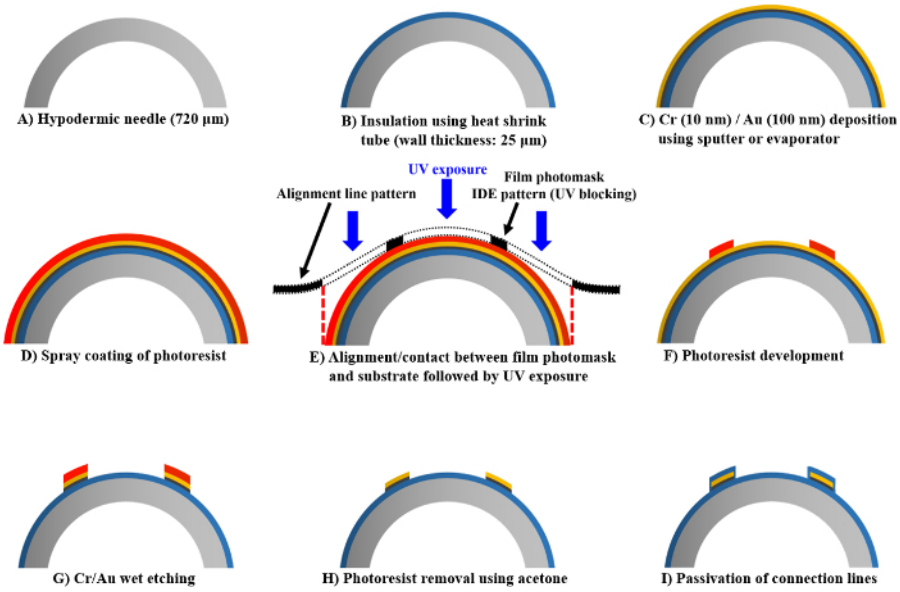

Figure 1: Schematic of overall EIS-on-a-needle (EoN) fabrication process. (A) Preparation of hypodermic needle, **(B)** Electrical insulation of hypodermic needle using heat shrink tube (HST, wall thickness: 25 µm), **(C)** Cr/Au deposition using sputtering or evaporator, **(D)** Spray coating of photoresist (positive type), **(E)** Alignment process of film photomask and photoresist-coated hypodermic needle followed by UV exposure.The film photomask includes patterns of interdigitated electrodes (IDEs) and alignment line, **(F)** development process, **(G)** Cr/Au wet etching, **(H)** Removal of residual photoresist using acetone, and **(I)** Passivation on connection lines using HST. Please click here to view a larger version of this figure.

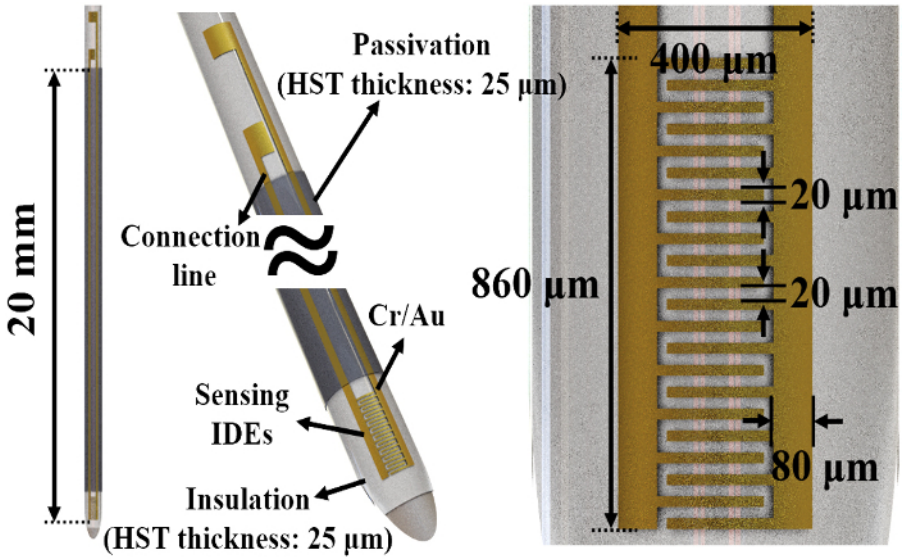

Figure 2: Detailed structural schematic of the EoN. The shape of the sensing electrodes was designed to be fine interdigitated electrodes to secure a larger effective sensing area on the limited surface of the hypodermic needle. A PET heat shrink tube (HST) was used as the electrical insulation layer for both the interdigitated electrodes (IDEs) and the connection lines, and was also used as the electrical passivation layer for the connection lines. Please click here to view a larger version of this figure.

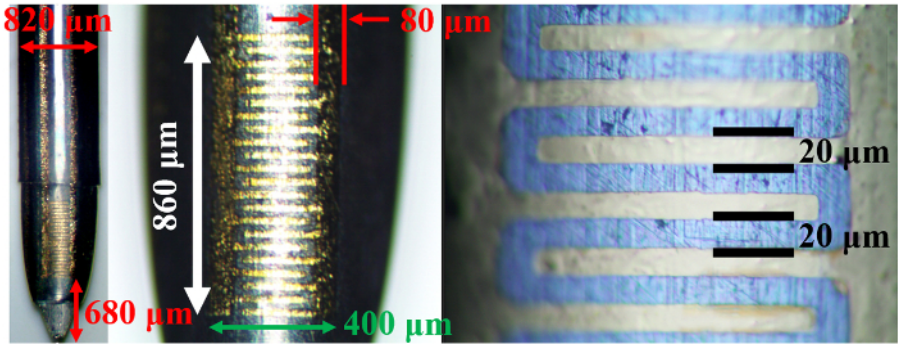

Figure 3: Microscopic images of the successfully fabricated EoN. Both the width and gap of the IDEs are as low as 20 µm. The overall length and width of the interdigitated electrodes (IDEs) are 860 µm and 400 µm, respectively. The fabrication margin from the tip is as small as 680 µm. Please click here to view a larger version of this figure.

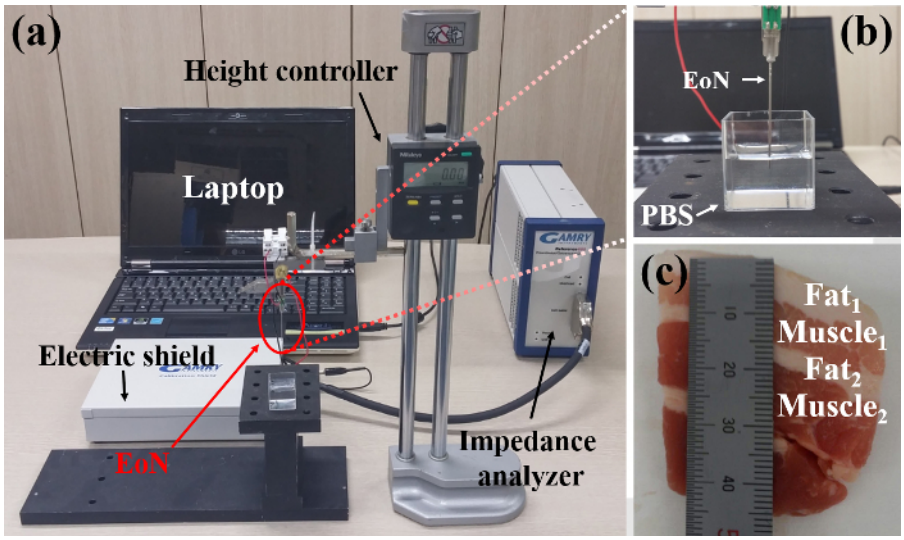

Figure 4: Images of experimental setup. To evaluate the discrimination capability of the EoN and its depth profiling capability into the biotissue, various concentration levels of PBS and four-layered porcine tissue were employed, respectively. To carry out depth profiling into the four-layered porcine tissue, the EoN was fixed on the height controller with a resolution of 10 µm. The various concentration levels of PBS were prepared as 1x, 0.5x, 0.25x, 0.125x, and 0.0625x, by serially diluting the 1x PBS with deionized (DI) water. (**a**) overall setup, (**b**) EoN immersed in the PBS, and (**c**) four-layered porcine tissue. This figure has been modified from the previously published study[23]. Please click here to view a larger version of this figure.

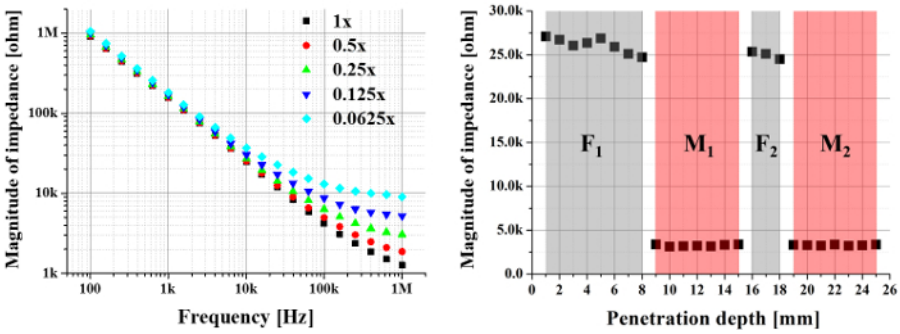

Figure 5: Experimental results using PBS and four-layered porcine tissue. Evaluation of the discrimination capability of EoN using (**a**) various concentration levels of PBS and (**b**) four-layered porcine tissue. Because the 1x PBS was diluted serially with DI water, the electrical conductivity of diluted PBS decreased with increased dilution because of the low conductivity of DI water. Thus, the magnitude of impedance increased as the concentration level of PBS decreased. The depth profiling of the porcine tissue was carried out at the frequency of 1 MHz, which was determined to be the optimal frequency in our previous study[23]. The magnitude of impedance measured from fat tissues was clearly discriminated from that of muscle tissues according to the penetration depth of the EoN. F1, F2, M1, and M2 represent fat1, fat2, muscle1, and muscle2 shown in **Figure 4** (**c**), respectively. This figure has been modified from the previously published study[23]. Please click here to view a larger version of this figure.

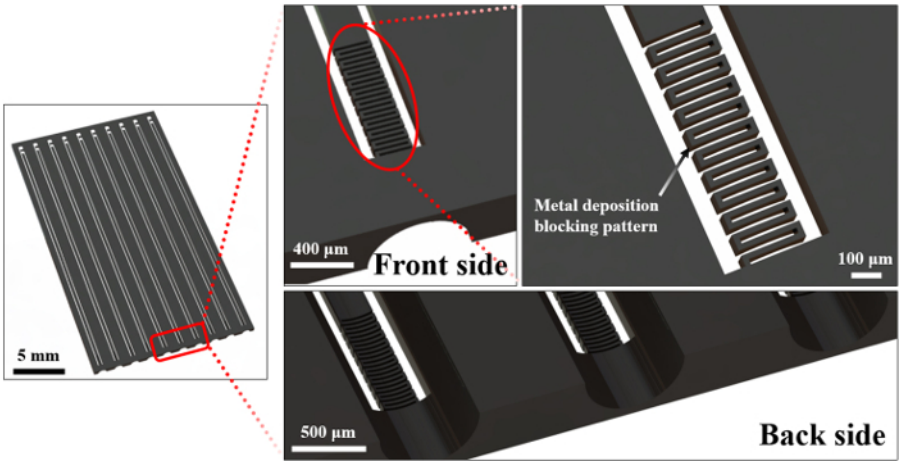

Figure 6: Schematic of a shadow mask to deposit metal electrodes for bulk production. The shadow mask can be made using a 3D printer with fine resolution. The shadow mask can physically block the area where metal deposition is unwanted during a physical deposition process, such as sputtering and/or evaporation. Please click here to view a larger version of this figure.

Discussion

We demonstrated that photolithography using spray coating and a film photomask is a feasible method to fabricate fine IDEs on the curved surface of a hypodermic needle with a small diameter of less than 1 mm. Both the width and the gap of the IDEs are as low as 20 µm, and the fabrication margin from the tip is as small as 680 µm. Within the protocol, the alignment process, including wedge error removal, is a critical step. The production yield was over 90% when the EoN was manufactured individually through a rigorous alignment process. This indicates that the proposed fabrication method has the potential to be developed for bulk production at an affordable price.

The discrimination capability of the EoN has been previously verified for PBS, porcine fat/muscle tissues, and even human renal tissues[6,23,24]. One clinical application is for surgery that involves the partial resection of tumors to preserve as much normal tissue as possible by detecting the surgical margin between the normal and lesion tissues[25]. Furthermore, the EoN is expected to be utilized in other clinical applications such as thyroid/prostate biopsies and anesthesia drug delivery in a spinal space.

Although the width and gap of the IDEs were fabricated to be 20 µm in the present study, they can be reduced to 10 µm once the resolution of printable film photomasks increases. Another way to reduce the dimensions of the gap and width of the IDEs is to transfer smaller patterns of a chrome mask to a flexible film using the photolithography process. Meanwhile, the wall thickness of the HST can be reduced from 25 µm to a smaller size that is commercially available. A smaller HST with a wall thickness of 6 µm was experimentally verified to be used for electrical insulation and the passivation layer using the same fabrication process. This will facilitate insertion experiments into animal tissues and even lessen the pain of patients in clinical use.

The fabrication method using the photolithography process can be developed for bulk production with a high yield at an affordable price by arranging many hypodermic needles together and by designing a photomask array. Another feasible method for bulk production is to use an array of shadow mask molds made by a 3D printer with high resolution as shown in **Figure 6**. The shadow mask can physically block the area where metal deposition is unwanted during a physical deposition process, such as sputtering and/or evaporation. Cr/Au deposited on the shadow mask can be readily removed using Cr/Au wet etchant for reuse of the shadow mask. The expected limitations to be addressed are as follows: 1) a 3D printer with high resolution is required, 2) the materials used in the 3D printer should be chemically resistant to the Cr/Au wet etchant for reuse of the shadow mask, and 3) the materials used in the 3D printer should not deform at temperatures above 150 °C that might be induced during the sputtering process. The next plan of the present study is to develop the bulk production method at an affordable price and to verify the applicability of the EoN in spinal anesthesia and thyroid/prostate biopsies.

Disclosures

The authors have nothing to disclose.

Acknowledgements

This work was supported by the "Biomedical Integrated Technology Research" project through a grant provided by GIST in 2017.

References

1. Knappe, M., Louw, M., & Gregor, R. T. Ultrasonography-guided fine-needle aspiration for the assessment of cervical metastases. *Arch Otolaryngol Head Neck Surg.* **126** (9), 1091-1096 (2000).
2. Paladini, D. Sonography in obese and overweight pregnant women: clinical, medicolegal and technical issues. *Ultrasound Obstet Gynecol.* **33** (6), 720-729 (2009).

3. Okuda, Y., Mishio, M., Kitajima, T., & Asai, T. Cremasteric reflex test as an objective indicator of spinal anaesthesia. *Anaesthesia.* **55** (6), 587-589 (2000).
4. Pryle, B., Carter, J., & Cadoux-Hudson, T. Delayed paraplegia following spinal anaesthesia. *Anaesthesia.* **51** (3), 263-265 (1996).
5. SJÖSTRÖMand, S., & Bläss, J. Severe pain in both legs after spinal anaesthesia with hyperbaric 5% lignocaine solution. *Anaesthesia.* **49** (8), 700-702 (1994).
6. Yun, J. *et al.* Electrochemical impedance spectroscopy with interdigitated electrodes at the end of hypodermic needle for depth profiling of biotissues. *Sens Actuator B-Chem.* **237** 984-991 (2016).
7. Ye, W. W., Shi, J. Y., Chan, C. Y., Zhang, Y., & Yang, M. A nanoporous membrane based impedance sensing platform for DNA sensing with gold nanoparticle amplification. *Sens Actuator B-Chem.* **193** 877-882 (2014).
8. Wang, L. *et al.* A novel electrochemical biosensor based on dynamic polymerase-extending hybridization for E. coli O157: H7 DNA detection. *Talanta.* **78** (3), 647-652 (2009).
9. Tran, H. *et al.* An electrochemical ELISA-like immunosensor for miRNAs detection based on screen-printed gold electrodes modified with reduced graphene oxide and carbon nanotubes. *Biosens Bioelectron.* **62** 25-30 (2014).
10. Nguyen, B. T. *et al.* Membrane-based electrochemical nanobiosensor for the detection of virus. *Anal Chem.* **81** (17), 7226-7234 (2009).
11. Tian, F., Lyu, J., Shi, J., Tan, F., & Yang, M. A polymeric microfluidic device integrated with nanoporous alumina membranes for simultaneous detection of multiple foodborne pathogens. *Sens Actuator B-Chem.* **225** 312-318 (2016).
12. Chan, K. Y. *et al.* Ultrasensitive detection of E. coli O157: H7 with biofunctional magnetic bead concentration via nanoporous membrane based electrochemical immunosensor. *Biosens Bioelectron.* **41** 532-537 (2013).
13. Giaever, I., & Keese, C. R. A morphological biosensor for mammalian cells. *Nature.* **366** (6455), 591 (1993).
14. Lu, Y.-Y., Huang, J.-J., Huang, Y.-J., & Cheng, K.-S. Cell growth characterization using multi-electrode bioimpedance spectroscopy. *Meas Sci Technol.* **24** (3), 035701 (2013).
15. Müller, J., Thirion, C., & Pfaffl, M. W. Electric cell-substrate impedance sensing (ECIS) based real-time measurement of titer dependent cytotoxicity induced by adenoviral vectors in an IPI-2I cell culture model. *Biosens Bioelectron.* **26** (5), 2000-2005 (2011).
16. Nordberg, R. C. *et al.* Electrical Cell-Substrate Impedance Spectroscopy Can Monitor Age-Grouped Human Adipose Stem Cell Variability During Osteogenic Differentiation. *Stem Cells Transl Med.* sctm. 2015-0404 (2016).
17. Messina, W., Fitzgerald, M., & Moore, E. SEM and ECIS Investigation of Cells Cultured on Nanopillar Modified Interdigitated Impedance Electrodes for Analysis of Cell Growth and Cytotoxicity of Potential Anticancer Drugs. *Electroanalysis.* **28** (9), 2188-2195 (2016).
18. Abdolahad, M. *et al.* Single-cell resolution diagnosis of cancer cells by carbon nanotube electrical spectroscopy. *Nanoscale.* **5** (8), 3421-3427 (2013).
19. Lee, H. *et al.* An endoscope with integrated transparent bioelectronics and theranostic nanoparticles for colon cancer treatment. *Nat Commun.* **6** 10059-10059 (2014).
20. Haemmerich, D., Schutt, D. J., Wright, A. S., Webster, J. G., & Mahvi, D. M. Electrical conductivity measurement of excised human metastatic liver tumours before and after thermal ablation. *Physiol Meas.* **30** (5), 459 (2009).
21. Prakash, S. *et al.* Ex vivo electrical impedance measurements on excised hepatic tissue from human patients with metastatic colorectal cancer. *Physiol Meas.* **36** (2), 315 (2015).
22. Yun, J., Kim, H. W., Kim, H.-I., & Lee, J.-H. Electrical impedance spectroscopy on a needle for safer Veress needle insertion during laparoscopic surgery. *Sens Actuator B-Chem.* **250** 453-460 (2017).
23. Yun, J., Kim, H. W., & Lee, J.-H. Improvement of Depth Profiling into Biotissues Using Micro Electrical Impedance Spectroscopy on a Needle with Selective Passivation. *Sensors.* **16** (12), 2207 (2016).
24. Yun, J. *et al.* Micro electrical impedance spectroscopy on a needle for ex vivo discrimination between human normal and cancer renal tissues. *Biomicrofluidics.* **10** (3), 034109 (2016).
25. Kim, H. W., Yun, J., Lee, J. Z., Shin, D. G., & Lee, J. H. Evaluation of Electrical Impedance Spectroscopy-on-a-Needle as a Novel Tool to Determine Optimal Surgical Margin in Partial Nephrectomy. *Adv Healthc Mater.* (2017).
26. Wu, H. *et al.* Conformal Pad-Printing Electrically Conductive Composites onto Thermoplastic Hemispheres: Toward Sustainable Fabrication of 3-Cents Volumetric Electrically Small Antennas. *PLoS One.* **10** (8), e0136939 (2015).
27. Ahn, C. *et al.* Direct fabrication of thin film gold resistance temperature detection sensors on a curved surface using a flexible dry film photoresist and their calibration up to 450° C. *J Micromech Microeng.* **23** (6), 065031 (2013).
28. Goluch, E. D. *et al.* Microfluidic method for in-situ deposition and precision patterning of thin-film metals on curved surfaces. *Appl Phys Lett.* **85** (16), 3629-3631 (2004).
29. Hu, X. *et al.* A degradable polycyclic cross-linker for UV-curing nanoimprint lithography. *J Mater Chem C.* **2** (10), 1836-1843 (2014).
30. Wu, J.-T., Lai, H.-C., Yang, S.-Y., Huang, T.-C., & Wu, S.-H. Dip coating cooperated with stepped rotating lithography to fabricate rigid microstructures onto a metal roller. *Microelectron Eng.* **87** (11), 2091-2096 (2010).

